Poll Res. 42 (2) : 188-197 (2023)

ISSN 0257–8050

DOI No.: http://doi.org/10.53550/PR.2023.v42i02.002

ABATEMENT OF HARMFUL CARBON MONOXIDE OVER THE NICKLE DOPED CO_3O_4 CATALYST

CHIU-HUNG LIU[1], MIN-CHUN SIE[2], CHIH-WEI TANG[3] AND CHEN-BIN WANG[2,4*]

[1]Graduate School of National Defense Science, Chung Cheng Institute of Technology, National Defense University, Taoyuan, 33509, Taiwan, ROC

[2]Department of Chemical and Materials Engineering, Chung Cheng Institute of Technology, National Defense University, Taoyuan, 33509, Taiwan, ROC

[3]Department of General Education, Army Academy ROC, Taoyuan, 32092, Taiwan, ROC

[4]Undergraduate Degree Program of System Engineering and Technology, National Yang Ming Chiao Tung University, Hsinchu, 30010, Taiwan, ROC"

(Received 14 October, 2022; Accepted 7 December, 2022)

ABSTRACT

This work aimed at evaluating the effect of nickle (Ni) dopant on the catalytic performance of Co_3O_4 catalyst for abatement of harmful carbon monoxide (CO), a resistance toward sintering and durability of catalytic activity were also pursued. Choose the $Co(NO_3)_2{\times}6H_2O_{(aq)}$ as precursor and NaOH as precipitant to prepare cobalt oxide (Co_3O_4) with precipitation method, then calcined at 300 and 500 °C, separately (named as C3 and C5). The Ni dopant (0.1 ~ 5 wt%) was added by deposited precipitation through $Ni(NO_3)_2{\times}6H_2O_{(aq)}$ with drop wisely added $NaOH_{(aq)}$ into suspended Co_3O_4 solution, then put the NaOCl for oxidation to obtain series 0.1%Ni-Co_3O_4, 0.2%Ni-Co_3O_4, 1%Ni-Co_3O_4 and 5%Ni-Co_3O_4 catalysts. All catalysts were characterized through BET, XRD, TEM/SEM, Raman, ICP and TPR instruments, and evaluated the catalytic performance of CO oxidation with a self-devised fluidized micro-reactor. It was observed that the calcination temperature and loading of dopant remarkably influenced the physicochemical characteristics and catalytic performance of the catalysts. Preferential catalyst was obtained for calcination at 300 °C and loading of Ni dopant below 1%. The doping of Ni on the surface of Co_3O_4 enhanced the performance due to the inducing of synergistic effect between Co_3O_4 and NiO, while the excessive NiO incorporated to the surface constrained the activity due to the abundant NiO on the surface, overlaying the active sites caused the decreasing of surface area and reducible capacity. Among these series Ni-Co_3O_4 catalysts, the 0.2%Ni-Co_3O_4(C3) catalyst behaved an eminent activity with T_{50} of 98 °C and durability without apparent deactivation for 50 hr reaction at 125 °C. The excellent performance is primarily attributed to the synergistic effect and formation of $NiCo_2O_4$ composite oxide.

KEY WORDS : Co_3O_4, Ni dopant, Harmful CO abatement, Catalytic performance.

INTRODUCTION

Harmful carbon monoxide (CO) is an odorless, colorless, and suffocating gas, which can cause poisoning as the content in air exceeds 1000 ppm (Xu *et al.*, 2020). In order to ensure the safety of living and working areas, it is very important to eliminate trace amounts of CO in the environment. In general, to devise innovational catalyst for the treatment of CO under low temperatures catalytic oxidation is a great pursuit in academia and industry (Schryer *et al.*, 1991; Royer and Duprez, 2011; Li *et al.*, 2014). Nowadays, supported noble-metal catalysts are well-known for the low-temperature CO catalytic oxidation (Grabchenko *et al.*, 2020; Zhang *et al.*, 2019; Zhang *et al.*, 2019; Fujita *et al.*, 2019; Khder *et al.*, 2019; Ha *et al.*, 2018; Panagiotopoulou and Verykios, 2017; Zhang *et al.*, 2015; Haruta, 2011). The noble metals include Au (Li *et al.*, 2014; Fujita *et al.*, 2019; Ha *et al.*, 2018; Haruta,

2011), Ag (Grabchenko *et al.*, 2020), Pt (Schryer *et al.*, 1991; Zhang *et al.*, 2019), Rh (Zhang *et al.*, 2019), Pd (Khder *et al.*, 2019), Ru (Panagiotopoulou and Verykios, 2017) and Ir (Zhang *et al.*, 2015) etc, and the supports incorporate Al_2O_3 (Lou and Liu, 2017; Comotti *et al.*, 2006), SiO_2 (Dutov *et al.*, 2016; Jung *et al.*, 2014), TiO_2 (Li *et al.*, 2014; Panagiotopoulou and Verykios, 2017), ZnO (Fujita *et al.*, 2019; Han *et al.*, 2019), ZrO_2 (Comotti *et al.*, 2006; Li *et al.*, 2020), FeO_x (Zhang *et al.*, 2015; Lou and Liu, 2017), Co_3O_4 (Huang *et al.*, 2020; Yu *et al.*, 2013), MnO_x (Zhang *et al.*, 2019; Khder *et al.*, 2019), CeO_2 (Li *et al.*, 2014; Grabchenko *et al.*, 2020; Ha *et al.*, 2018), $CeZrLaO_x$ (Yang *et al.*, 2016), $Ce_xZr_{1-x}O_2$ (Li *et al.*, 2020; Valechha *et al.*, 2017), ZSM-5 (Kolobova *et al.*, 2017) and SBA-15 (Zhang *et al.*, 2016) etc. In general, in order to enhance the activity of CO oxidation, the active ingredients must be uniformly dispersed on the carrier. However, apart from the high cost of series supported noble-metal catalysts, there are also problems of nanoparticle sintering and susceptible poisoning of catalyst to restrict their wide applications.

Over the last couple of decades, transition metal oxides have been manifested as heterogeneous catalysts and possess potential for low temperature catalytic activity for harmful CO oxidation (Jansson, 2000; Jansson *et al.*, 2002; Lin *et al.*, 2003; Wang *et al.*, 2005). Cobalt oxide (Co_3O_4) (Jansson *et al.*, 2002; Yu *et al.*, 2009; Molavi *et al.*, 2021) and manganese oxides (MnO, Mn_3O_4, Mn_2O_3 and MnO_2) (Dey and Kumar, 2020; Frey *et al.*, 2012) are the most brilliant candidates owing to the reducible mobile oxygen on the surface to weaken the Co-O and/or Mn-O bond, which easily releases the species of active oxygen or mobile lattice oxygen simultaneously with formation of oxygen vacancies. And next for the CuO and NiO (Royer and Duprez, 2011; Yu *et al.*, 2009) on the CO catalytic oxidation among these transition metal oxides. However, the performance of bulk Co_3O_4 is still deficient. It has been displayed that increasing the specific surface area or decreasing the particle size could ameliorate the activity of Co_3O_4 (Zhu *et al.*, 2013; Bai *et al.*, 2013). Modification of catalyst also includes composite oxides with another metal oxide via the synergistic effects to enhance the activity (Faure and Alphonse, 2016; Xu *et al.*, 2015) or doping the trace elements (Cai *et al.*, 2018; Carabineiro *et al.*, 2015) via the mutual interaction to get high dispersion of oxide phases.

The present work gives an account of the effect of Ni-doping in Co_3O_4 catalyst using the deposited precipitation (DP) coupled with oxidation method, and verifies the catalytic oxidation of harmful CO at different temperatures under atmospheric pressure. The discussed parameters include the calcination temperature and loading of Ni dopant.

MATERIALS AND METHODS

Preparation of catalysts

All reagents were purchased and used directly without further purified. Choose the $Co(NO_3)_2{\times}6H_2O$ (Showa, 98%, 0.16 mol) as precursor and NaOH (Ferak, 3.2 M) as precipitant with precipitation method, then calcined at 300 and 500 °C, separately to obtain the cobalt oxide (Co_3O_4) (named as C3 and C5). The Ni-doped (0.1 ~ 5 wt%) Co_3O_4 was fabricated by deposited precipitation through $Ni(NO_3)_2{\times}6H_2O$ (Showa, 98%) with dropwisely added $NaOH_{(aq)}$ into the previously prepared suspended Co_3O_4 solution, then put the $NaOCl_{(aq)}$ (Showa, 12%) oxidant for oxidation to obtain series as-prepared precursors, then calcined at 300 and/or 500 °C for 4 hr to get series 0.1%Ni-Co_3O_4, 0.2%Ni-Co_3O_4, 1%Ni-Co_3O_4 and 5% Ni-Co_3O_4 catalysts.

Characterization

The X-ray diffraction (XRD) profiles of the series catalysts were carried out using a Bruker, D2 Phaser diffractometer. The patterns were run (scanning speed of $2°{\times}min^{-1}$) with a Ni-filtered Cu $K_{á1}$ radiation (λ = 0.154 nm) at 30 mA and 40 kV, in the diffraction angle (2θ) range 10 - 90°. Further, the crystallite sizes of catalysts were calculated with the Scherrer equation. Surface area of catalysts was measured through the nitrogen physisorption at 77 K in the relative pressure range of 0.05 - 0.3 with a Quantachrome Autosorb-1 apparatus and calculated with BET equation. Morphology and elemental distribution on the surface of catalyst was inspected by scanning electron microscopy (SEM, JEOL, JSM-7100F) coupled with energy dispersive spectroscopy (EDS). Particle size of catalysts was analyzed by transmission electron microscopy (TEM JEOL JEM-2010; HRTEM–FEI Tecnai G2). Reduction feature of catalysts was surveyed through the temperature-programmed reduction (TPR) coupled a thermal conductivity detector (TCD). During the TPR measurement, taking 25 mg sample and controlled the heating rate of 10 $°C{\times}min^{-1}$ to raise

from room temperature to 500 °C under a flowing 10% H_2/N_2 reducing gas with a flow rate of 10 mL×min^{-1}. Raman spectroscopy was measured by a Raman spectrometer (Horiba JY, LabRAM ARAMIS) using a diode laser emitted at 780 nm, and collected the spectrum between 100 and 1000 cm^{-1}.

Activity test

The harmful CO catalytic oxidation of series Ni-Co_3O_4 catalysts was executed in a self-devised fluidized fixed-bed reactor, and the mixed gas of 4% O_2/He with 1% CO/He was maintained a rate of 50 mL×min^{-1} to feed into a 0.02 g catalyst reactor during the reaction at atmospheric pressure. The reaction was regulated and warming up from room temperature to 200 °C under steady-state conditions at each captured temperature. The effluent gas stream was separated with a packed Carboxen-1000 column and resolved by using gas chromatography coupled with a thermal conductivity detector (TCD). The conversion of CO oxidation is calculated in accordance with the list equation.

$$\text{CO conversion (\%)} = ([CO]_{inlet} - [CO]_{outlet})/[CO]_{inlet} \times 100\%$$

Both the $[CO]_{inlet}$ and $[CO]_{outlet}$ are the initial and final concentration of CO.

RESULTS AND DISCUSSION

Characterization of catalysts

Physicochemical properties of NiO, Co_3O_4 and series Ni-Co_3O_4 catalysts are characterized and summarized in Table 1. The BET surface area (S_{BET}) (6th column of Table 1) indicates that both Co_3O_4(C3) and 0.2%Ni-Co_3O_4(C3) present larger surface area (nears 30 m^2×g^{-1}) among series catalysts (others below 20 m^2×g^{-1}). Simultaneously, the particle size (7th column of Table 1) is fluctuated with the calcined temperature and the amount of Ni dopant. Apparently, in addition to the amounts of Ni dopant, also, the calcined temperature can influence the physicochemical properties. Furthermore, the particle size of Co_3O_4 is small than the series Ni-Co_3O_4 catalysts which is attributed the secondary calcination for Ni-Co_3O_4 samples under the preparation of catalyst. While, appropriate tune of dopant can obtain a catalyst with a high surface area. The XRD patterns of NiO, Co_3O_4 and series Ni-Co_3O_4 catalysts are shown in Figure 1. For pure NiO, the diffraction peaks at 2θ = 37.4°, 43.5°, 63.1°, 75.7° and 79.6°, corresponding to (111), (200), (220), (311) and (222) planes, respectively, are attributed to the cubic NiO (JCPDS 1-1239). The diffraction peaks of pure Co_3O_4 at 2θ = 19.2°, 31.6°, 37.2°, 38.8°, 45.2°, 56.3°, 59.7° and 63.6°, corresponding to (111), (220), (311), (222), (400), (422), (511) and (440) planes, respectively, are ascribed to the spinel Co_3O_4 (JCPDS 65-3103). With increasing the calcined temperature, the growth of crystalline phase and a decreasing of surface area could be noticed. According to the width of diffraction peaks and calculated the particle size with Scherrer equation, it can be seen that the peak of Co_3O_4(C5) is narrow and sharper than Co_3O_4(C3), indicating a larger crystal size of Co_3O_4(C5) (17.1 nm) than the Co_3O_4(C3) (12.5 nm), also the same tendency is observed on Ni-Co_3O_4 catalysts, i.e. 19.3 nm and 26.3 nm for 0.2%Ni-Co_3O_4(C3) and 0.2%Ni-Co_3O_4(C5), respectively. The main diffraction peaks of series Ni-Co_3O_4 catalysts [Figure 1(B)] display a spinel Co_3O_4 phase with faint

Table 1. Characterization and catalytic activity of CO oxidation over series Ni-Co_3O_4 catalysts

Samples	T_C(°C)[a]	TPR (°C)[b]			S_{BET}	d_{Co3O4} (nm)		T_{50}(°C)[d]
		T_i	T_1	T_2	(m^2×g^{-1})	Fresh	Used	
			NiO and Co_3O_4 catalysts					
NiO(C5)	500	246	259	341	20	18[c]	18[c]	189
Co_3O_4(C3)	300	207	284	348	30	13	15	110
Co_3O_4(C5)	500	227	317	360	18	17	24	114
			Ni-Co_3O_4 catalysts					
5%Ni-Co_3O_4(C3)	300	260	334	361	19	20	20	171
1%Ni-Co_3O_4(C3)	300	217	337	375	22	21	22	109
0.2%Ni-Co_3O_4(C5)	500	235	320	360	15	26	26	118
0.2%Ni-Co_3O_4(C3)	300	202	305	360	31	19	19	98
0.1%Ni-Co_3O_4(C3)	300	203	280	345	27	18	19	106

[a]: Calcined temperature
[b]: T_i is initial reduction; T_1 is $Co_3O_4 \xrightarrow{[H]} CoO$ or $NiO_X \xrightarrow{[H]} NiO$; T_2 is $CoO \xrightarrow{[H]} Co^{or}$ $NiO \xrightarrow{[H]} Ni$
[c]:Particle size of NiO[d]: Temperature of 50 % CO conversion

signal of NiO in all series samples which demonstrated that the doped Ni^{2+} may be incorporated into the lattice of Co_3O_4 and/or well-dispersed. The optimal 0.2%Ni-Co_3O_4(C3) catalyst possesses high surface area and small particle size in the series Ni-Co_3O_4 catalysts.

No doubt, the physicochemical properties of Ni-Co_3O_4 catalysts are strongly influenced by the calcination temperature and amounts of dopant. The grain growth of Co_3O_4 particle under thermal treatment becomes apparent at higher temperature (Shao *et al.*, 2007) to approach the low surface area and large particle size, and the optimal Ni dopant can disperse effectively the active species to get high surface area and small particle size.

Choose the TPR technique to demonstrate the reduction feature and further to comprehend the bond strength of metal oxides. Figure 2 exhibits the TPR profiles of NiO, Co_3O_4 and series Ni-Co_3O_4 catalysts. The initial reduction temperature (T_i) of Co_3O_4(C3) (207 °C) is lower than that of Co_3O_4(C5) (227 °C) [Figure 2(A)], which is due to the lower calcined temperature. Comparison with the particle size and surface area, the shift of T_i to a low temperature indicates that the dispersion and surface area of catalyst strongly affected the reduction property. The overlapped reduction peaks demonstrate that consecutive reduction of Co_3O_4 involves the Co_3O_4 reduced to CoO (T_1), and followed the CoO reduced to Co (T_2) (Zhang *et al.*, 2006). The initial reduction temperature of NiO (246 °C) is higher than that of Co_3O_4, and NiO also indicates two reduction peaks. The first step is attributed to the reduction of trace NiO_x to NiO, and

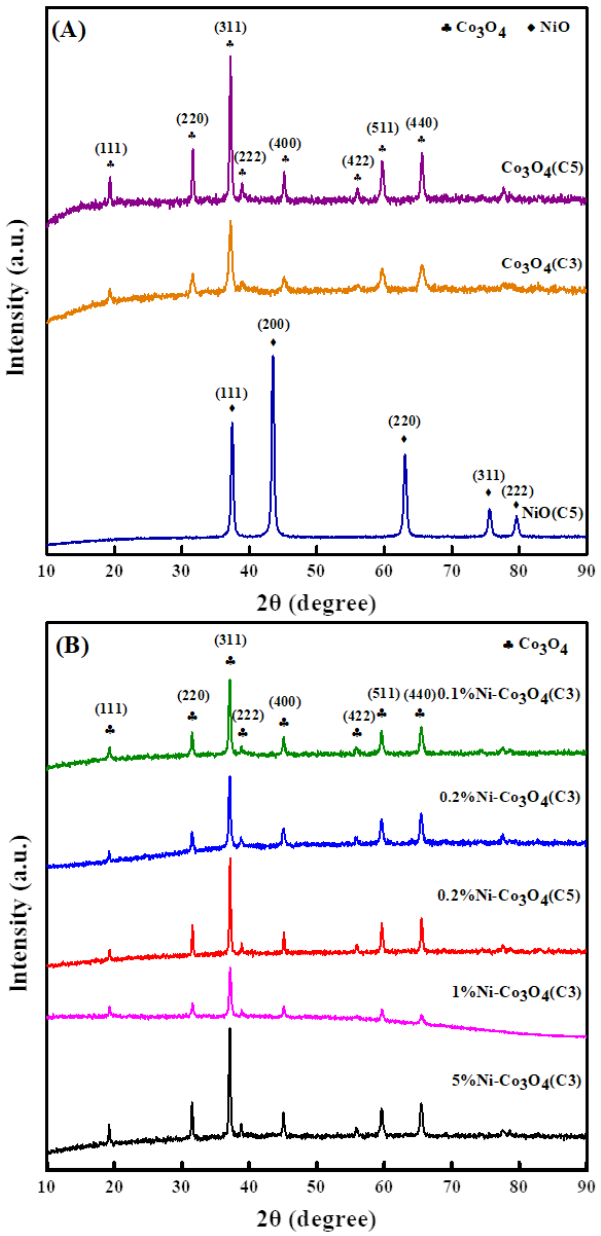

Fig. 1. XRD patterns of (A) NiO and Co_3O_4 (B) Ni-Co_3O_4 catalysts.

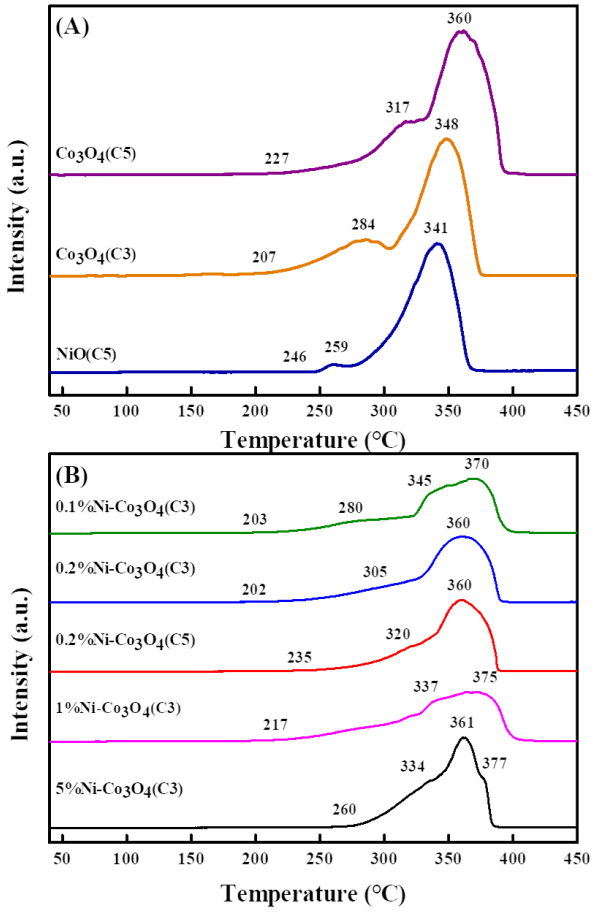

Fig. 2. TPR profiles of (A) NiO and Co_3O_4 (B) Ni-Co_3O_4 catalysts.

the second step belongs to reduce NiO to Ni metal (Lai *et al.*, 2009). The reduction of Ni-Co_3O_4 catalysts [Figure 2(B)] present similar to the Co_3O_4 profile. While, the doped Ni^{2+} may be incorporated into the lattice of Co_3O_4 and the dispersion depends on the amounts of dopant. Explicitly, the T_i decreases with the increase of Ni dopant, i.e. 203, 202, 217 and 260 °C for 0.1%Ni-Co_3O_4(C3), 0.2%Ni-Co_3O_4(C3), 1%Ni-Co_3O_4(C3) and 5%Ni-Co_3O_4(C3), respectively, owing to the lowering of reducible ability. As the Ni dopant less than 1% owns better dispersion, and become bad as the Ni dopant exceeds 1%. The sample of lower T_i can weaken the bond strength of Co–O and assists the desorption lattice oxygen from the Co_3O_4 surface to enhance the redox property of catalyst. We deduced that the lower T_i of the sample should be the sticking point on the CO oxidation performance.

The TEM images of Co_3O_4(C3), NiO(C3) and 0.2%Ni-Co_3O_4(C3) catalysts are shown in Figure 3. No obvious difference between the morphologies of Co_3O_4(C3) and NiO(C3). Both are constituted of several globular particles with crystallite size of 20 nm and 28 nm, respectively for Co_3O_4(C3) and NiO(C3), and indicates an agglomerated particles morphology. These particles are at least one and half times larger than the crystallite size calculated from XRD profiles. The image of 0.2%Ni-Co_3O_4(C3) catalyst shows that tiny NiO particles are attached to the surface of Co_3O_4, and there are a few film-like substances attached around the Co_3O_4, so it is difficult to reckon its particle size. Further, the HRTEM image of 0.2%Ni-Co_3O_4(C3) catalyst (Figure 4) clearly confirms that the microstructure of the attached globular NiO particles around the Co_3O_4 are homogeneously dispersed, and these nanoparticles reveal two lattice fringes with interplanar spacing of 0.245 and 0.208 nm, which corresponds to (311) and (400) of $NiCo_2O_4$ crystallographic facets (Yang *et al.*, 2016). Obviously, the lattice fringe of NiO do not observe, indicating that the doped Ni^{2+} indeed enters into Co_3O_4 lattice to form $NiCo_2O_4$ composite oxide. In the photocatalytic system for water splitting, Cheng et al (Cheng *et al.*, 2021) designed a novel $NiCo_2O_4$/g-C_3N_4 catalyst, and the related cooperative eect between $NiCo_2O_4$ and g-C_3N_4 can enhance the oxygen-evolution-reaction. According to this dissertation, we inferred that the formation of $NiCo_2O_4$ between the interface of NiO and Co_3O_4 can induce the catalytic activity on CO oxidation.

In order to further confirm that the doped Ni^{2+} enters into the Co_3O_4 lattice to form $NiCo_2O_4$ composite oxide, the formation and structural characteristics of the phases are identified by Raman spectroscopy. Figure 5 show the Raman spectra of 0.2%Ni-Co_3O_4(C3), 5%Ni-Co_3O_4(C3) and Co_3O_4(C3)

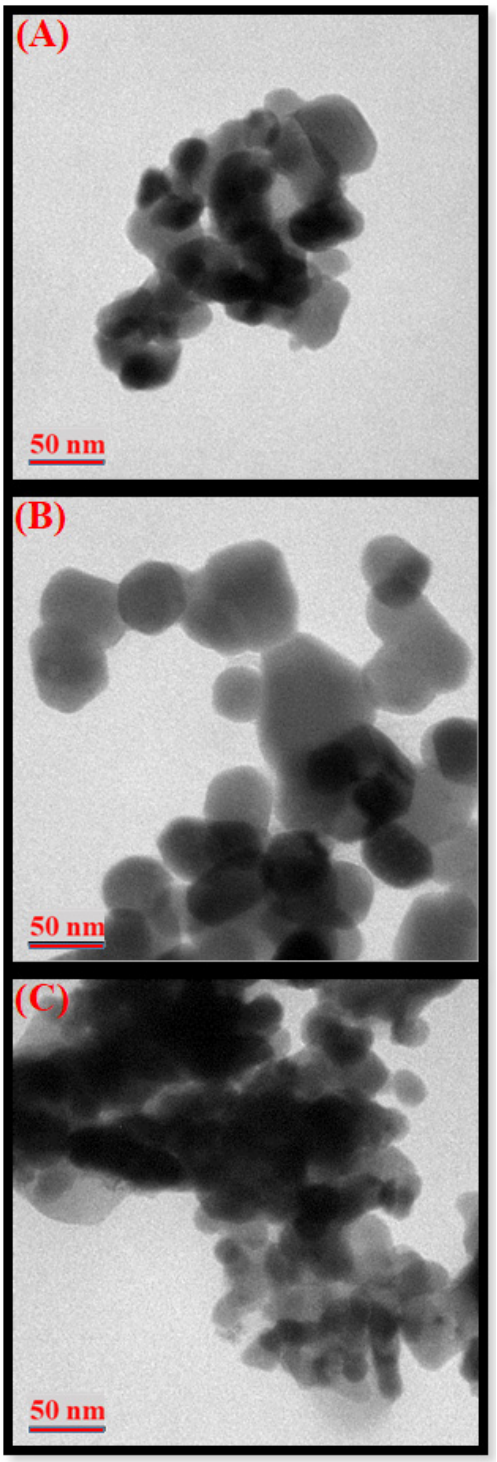

Fig. 3. TEM images of (A) Co_3O_4(C3) (B) NiO(C3) (C) 0.2%Ni-Co_3O_4(C3) catalysts.

catalysts. The Co_3O_4(C3) catalyst exhibits four Raman-active modes of A_{1g} (677 cm^{-1}), 2 F_{2g} (514 and 202 cm^{-1}) and E_g (478 cm^{-1}), which are consistent with the cubic spinel structure of Co_3O_4 (Chen *et al.*, 2017; Tang *et al.*, 2008). Raman-active modes of 0.2%Ni-Co_3O_4(C3) and 5%Ni-Co_3O_4(C3) are similar to that of Co_3O_4(C3) catalyst, except that the position of peaks is slightly shifted, which is attributed to the intercalated Ni–O and Co–O vibrations of the cubic spinel $NiCo_2O_4$. Among these, the A_{1g} mode shifts more obvious (677 to 660 cm^{-1}) since the charge transfer and/or electrostatic effect of octahedral sites Co^{3+} is substituted by the embedded Ni^{2+} species (Iliev *et al.*, 2013; Umeshbabu *et al.*, 2015). The identification of Raman spectra is consistent with HR-TEM, which affirms the $NiCo_2O_4$ phase.

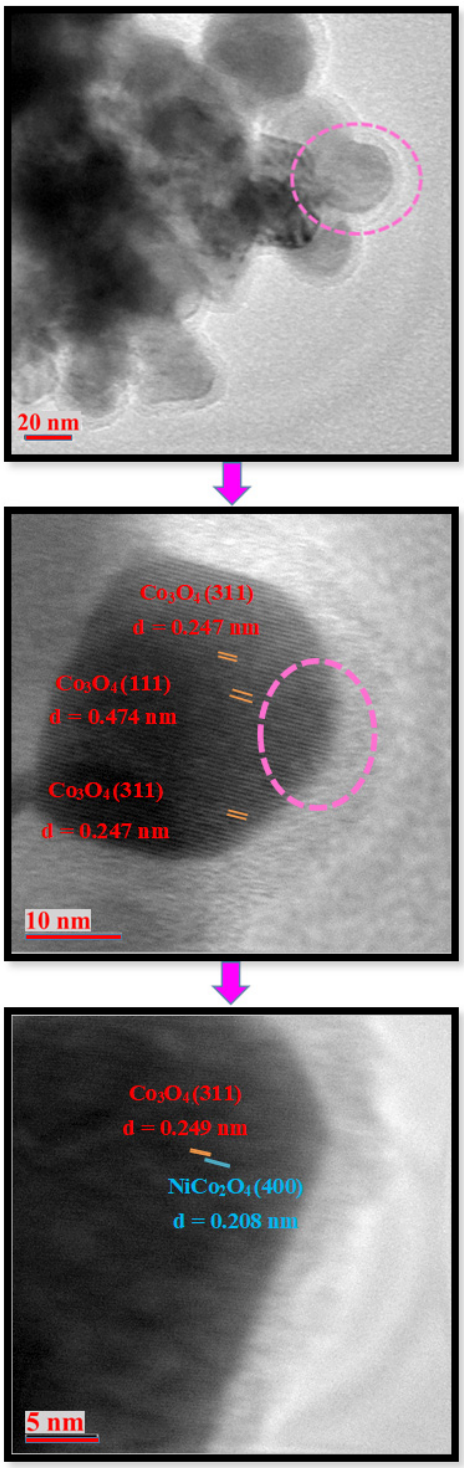

Fig. 4. HRTEM image of 0.2%Ni-Co_3O_4(C3) catalyst.

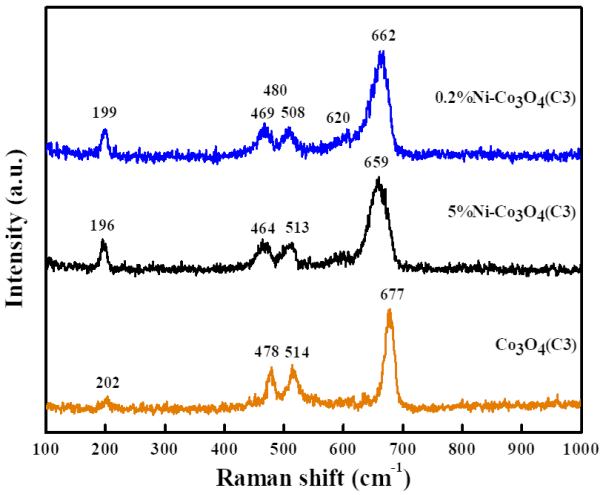

Fig. 5. Raman spectra of 0.2%Ni-Co_3O_4(C3), 5%Ni-Co_3O_4(C3) and Co_3O_4(C3) catalysts.

Evaluation of catalytic activity

The catalytic activity for harmful CO oxidation over NiO, Co_3O_4 and series Ni-Co_3O_4 catalysts is shown in Figure 6. All catalysts presented enhancing performance with temperature. Meanwhile, the activity of C_3O_4 is better than that of NiO, and the calcined pretreatment at 300 °C is better than that of 500 C. In addition, the amount of Ni dopant will also affect the activity. An appropriate amount of dopant is helpful for the dispersion of Co_3O_4. Also, the formation of $NiCo_2O_4$ composite oxide through the embedded of Ni^{2+} into the lattice of Co_3O_4, and the synergistic effect in the region of interface, which can enhance the catalytic activity. Zhong et al (Zhong *et al.*, 2014) found that the synergistic effect between $LaCoO_3$-Co_3O_4 system improved the performance of harmful CO oxidation. In the investigation of doping Co_3O_4 with ZnO, El-Shobaky and Ghozza (El-Shobaky and Ghozza, 2004) proposed the coordination effect between Co_3O_4 and ZnO can modify the concentration of active sites to improve the activity of CO oxidation. Manifestly, the

coordination effect can actuate the dispersion of Co_3O_4, effective formation of $NiCo_2O_4$ species and reducible capacity, which improve the catalytic performance of CO oxidation. Conversely, adding too little dopant will not effectively constitute composite oxide, adding too much dopant will reduce activity due to masking of active sites. The trend of T_{50} for harmful CO catalytic oxidation over series catalysts follows the order of NiO(C5) < 5%Ni-Co_3O_4(C3) < 0.2%Ni-Co3O4(C5) < Co_3O_4(C5) < Co_3O_4(C3) < 1%Ni-Co_3O_4(C3) < 0.1%Ni-Co_3O_4(C3) < 0.2%Ni-Co_3O_4(C3). Comparison with the physical and chemical characterizations, as the lower calcined temperature and Ni dopant less than 1% owns better activity since the well-dispersion and better reducible capacity, and become bad as the Ni dopant exceeds 1%.

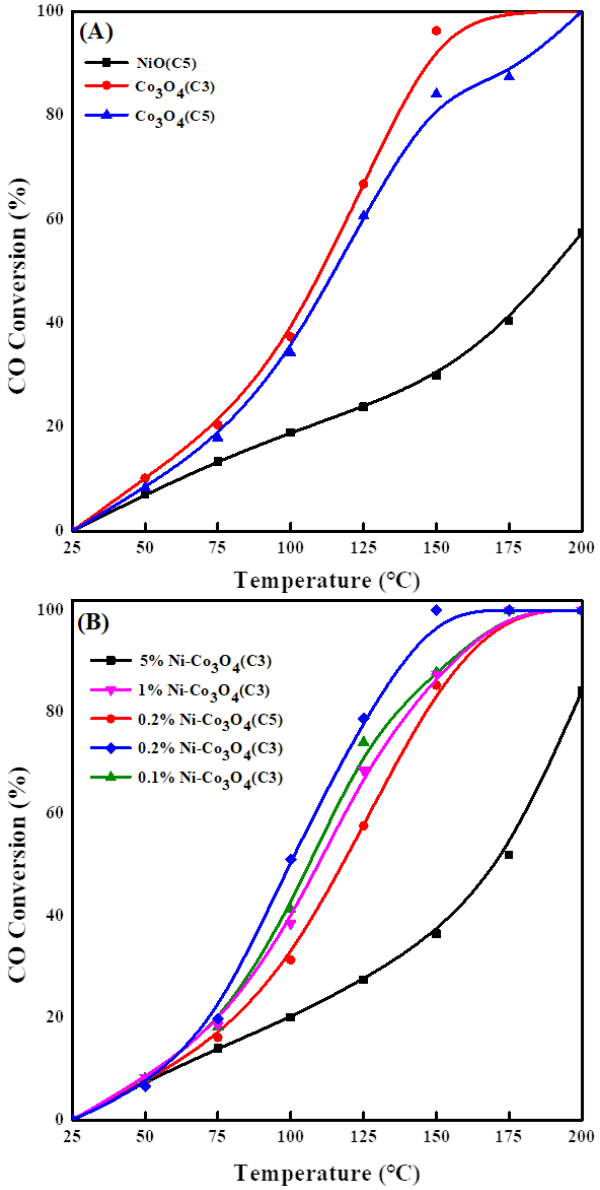

Fig. 6. Catalytic activity for CO oxidation over (A) NiO and Co_3O_4 (B) Ni-Co_3O_4 catalysts.

Catalytic activity and stability are important factors for evaluating the designed catalyst. The long-term stability of 0.2%Ni-Co_3O_4(C3) catalyst in the harmful CO oxidation reaction was carried out testing to confirm whether the catalyst possesses durability and thermal stability. To ensure reliable results, the temperature for CO oxidation was controlled at 125 °C (the initial activity approaches 80%). Figure 7 shows that the activity is stable, only a little decline of conversion (less than 4%). The catalyst still maintains catalytic activity for 50 hr, indicating that the catalyst behaves excellent durability in the CO oxidation. In general, the deactivation of catalyst is attributed to some factors, i.e. occupancy of moisture on active site, surface reconstruction and sintering of the catalyst (Vepøek *et al.*, 1986). Both XRD and TPR characterizations for fresh and used 0.2%Ni-Co_3O_4(C3) catalyst are shown in inset of Figure 7. Distinctly, the XRD patterns declare that the phase and crystallinity do not change. Also, the TPR profiles indicate tiny variation of reduction peak for the spent catalyst, which indicates that the surface reconstruction may be chanced with liable reduction to preserve the catalytic activity. Based on the tiny variations, further confirmed that the catalyst is a favorable candidate for low-temperature CO oxidation.

CONCLUSION

A series of Ni-Co_3O_4 catalysts with Ni dopant was

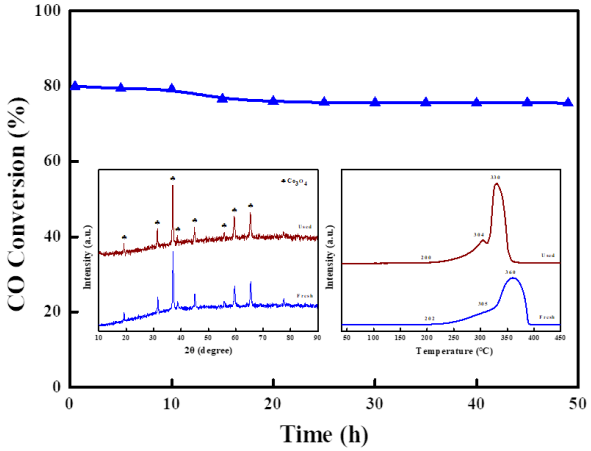

Fig. 7. Durability test of CO oxidation over 0.2%Ni-Co_3O_4(C3) catalyst at 125 °C (inset is the XRD patterns and TPR profiles of fresh and used catalyst).

fabricated and characterized. Integrated XRD, TPR, HRTEM and Raman characterizations revealed that the synergetic effect can actuate the dispersion of Co_3O_4, effective incorporated the Ni^{2+} into the lattice of Co_3O_4 to form $NiCo_2O_4$ species and tunes the reducible capacity, which improve the catalytic performance of harmful CO oxidation. The 0.2%Ni-Co_3O_4(C3) behaved an eminent activity among series Ni-Co_3O_4 catalysts for harmful CO oxidation with T_{50} of 98 °C and excellent durability without apparent deactivation for 50 hr reaction at 125 °C.

ACKNOWLEDGEMENT

The financial support of this work by the Ministry of Science and Technology (MOST 107-2113-M-606-001-), Taiwan is gratefully acknowledged.

Conflict of interest

We declare that we have no conflicts of interest to this work.

REFERENCES

Bai, B., Arandiyan, H. and Li, J. 2013. Comparison of the performance for oxidation of formaldehyde on nano-Co_3O_4, 2D-Co_3O_4, and 3D-Co_3O_4 catalysts. *Appl. Catal. B. Environ.* 142-143: 677-683.

Cai, J., Zhang, J., Cao, K., Gong, M., Lang, Y., Liu, X., Chu, S., Shan, B. and Chen, R. 2018. Selective passivation of Pt nanoparticles with enhanced sintering resistance and activity toward CO oxidation via atomic layer deposition. *ACS Appl. Nano. Mater.* 1(2): 522-530.

Carabineiro, S.A.C., Chen, X., Konsolakis, M., Psarras, A.C., Tavares, P.B., Órfão, J.J.M., Pereira, M.F.R. and Figueiredo, J.L. 2015. Catalytic oxidation of toluene on Ce-Co and La-Co mixed oxides synthesized by exotemplating and evaporation methods. *Catal. Today*. 244: 161-171.

Chen, J.C., Du, H.W., Zhang, J.H., Lei, X.R., Wang, Y., Su, S., Zhang, Z.H. and Zhao, P. 2017. Influence of deposition temperature on crystalline structure and morphologies of Co_3O_4 films prepared by a direct liquid injection chemical vapor deposition. *Surf. Coat Technol.* 319: 110-116.

Cheng, C., Mao, L.H., Shi, J.W., Xue, F., Zong, S.C., Zheng, B.T. and Guo, L.J. 2021. $NiCo_2O_4$ nanosheets as a novel oxygen-evolution-reaction cocatalyst in situ bonded on the g-C_3N_4 photocatalyst for excellent overall water splitting. *J. Mater. Chem. A.* 9: 12299-12306.

Comotti, M., Li, W.C., Spliethoff, B. and Schüth, F. 2006. Support effect in high activity gold catalysts for CO oxidation. *J. Am. Chem. Soc.* 128(3): 917-924.

Dey, S. and Kumar, V.V.P. 2020. The performance of highly active manganese oxide catalysts for ambient conditions carbon monoxide oxidation. *Cur. Res. Green Sustain. Chem.* 3: 100012.

Dutov, V.V., Mamontov, G.V., Zaikovskii, V.I. and Vodyankina, O.V. 2016. The effect of support pretreatment on activity of Ag/SiO_2 catalysts in low-temperature CO oxidation. *Catal. Today*. 278: 150-156.

El-Shobaky, G.A. and Ghozza, A.M. 2004. Effect of ZnO doping on surface and catalytic properties of NiO and Co_3O_4 solids. *Mater. Lett.* 58(5): 699-705.

Faure, B. and Alphonse, P. 2016. Co-Mn-oxide spinel catalysts for CO and propane oxidation at mild temperature. *Appl. Catal. B. Environ.* 180: 715-725.

Frey. K., Iablokov, V., Sáfrán, G., Osán, J., Sajó. I., Szukiewicz, R., Chenakin, S. and Kruse, N. 2012. Nanostructured MnO_x as highly active catalyst for CO oxidation. *J. Catal.* 287: 30-36.

Fujita, T., Ishida, T., Shibamoto, K., Honma, T., Ohashi, H., Murayama, T. and Haruta, M. 2019. CO oxidation over Au/ZnO: unprecedented change of the reaction mechanism at low temperature caused by a different O_2 activation process. *ACS Catal.* 9(9): 8364-8372.

Grabchenko, M.V., Mamontov, G.V., Zaikovskii, V.I., La Parola V, Liotta L.F. and Vodyankina, O.V. 2020. The role of metal-support interaction in Ag/CeO_2 catalysts for CO and soot oxidation. *Appl. Catal. B. Environ.* 260 : 118-148.

Ha, H., Yoon, S., An, K. and Kim, H.Y. 2018. Catalytic CO oxidation over Au nanoparticles supported on CeO_2 nanocrystals: effect of the Au-CeO_2 interface. *ACS Catal.* 8(12): 11491-11501.

Han, B., Lang, R., Tang, H., Xu, J., Gu, X.K., Qiao, B. and Liu, J(J). 2019. Superior activity of Rh_1/ZnO single-atom catalyst for CO oxidation. *Chin. J. Catal.* 40(12): 1847-1853.

Haruta, M. 2011. Role of perimeter interfaces in catalysis by gold nanoparticles. *Faraday Discuss.* 152: 11-32.

Huang, R., Kim, K., Kim, H.J., Jang, M.G. and Han, J.W. 2020. Size-controlled Pd nanoparticles loaded on Co_3O_4 nanoparticles by calcination for enhanced CO oxidation. *ACS Appl. Nano. Mater.* 3(1): 486-495.

Iliev, M.N., Silwal, P., Loukya, B., Datta, R., Kim, D.H., Todorov, N.D., Pachauri, N. and Gupta, A. 2013. Raman studies of cation distribution and thermal stability of epitaxial spinel $NiCo_2O_4$ films. *J. Appl. Phys.* 114(3): 033514/1-033514/5.

Jansson, J. 2000. Low-Temperature CO oxidation over Co_3O_4/Al_2O_3. *J. Catal.* 194: 55-60.

Jansson, J., Palmqvist, A.E.C., Fridell, E., Skoglundh, M., Österlund, L., Thormählen, P. and Langer, V. 2002. On the catalytic activity of Co_3O_4 in low-temperature CO oxidation. *J. Catal.* 211: 387-397.

Jung, C.H., Yun, J., Qadir, K., Naik, B., Yun, J.Y. and Park, J.Y. 2014. Catalytic activity of Pt/SiO_2 nanocatalysts synthesized via ultrasonic spray pyrolysis process under CO oxidation. *Appl. Catal. B. Environ.* 154/155 : 171-176.

Khder, A.E.R.S., Altass, H.M., Orif, M.I., Ashour, S.S. and Almazroai, L.S. 2019. Preparation and characterization of highly active Pd nanoparticles supported Mn_3O_4 catalyst for low-temperature CO oxidation. *Mater. Res. Bull.* 113: 215-222.

Kolobova, E., Pestryakov, A., Mamontov, G., Kotolevich, Y., Bogdanchikova, N., Farias, M., Vosmerikov, A., Vosmerikova, L. and Cortes Corberan, V. 2017. Low-temperature CO oxidation on Ag/ZSM-5 catalysts: influence of Si/Al ratio and redox pretreatments on formation of silver active sites. *Fuel.* 188: 121-131.

Lai, T.L., Lai, Y.L., Yu, J.W., Shu, Y.Y. and Wang, C.B. 2009. Microwave-assisted hydrothermal synthesis of coralloid nanostructured nickel hydroxide hydrate and thermal conversion to nickel oxide. *Mater. Res. Bull.* 44: 2040-2044.

Li, H., Shen, M., Wang, J., Wang, H. and Wang, J. 2020. Effect of support on CO oxidation performance over the Pd/CeO_2 and Pd/CeO_2-ZrO_2 catalyst. *Ind. Eng. Chem. Res.* 59(4): 1477-1486.

Li, S., Zhu, H., Qin, Z., Wang, G., Zhang, Y., Wu, Z., Li, Z., Chen, G., Dong, W., Wu, Z., Zheng, L., Zhang, J., Hu, T. and Wang, J. 2014. Morphologic effects of nano CeO_2-TiO_2 on the performance of Au/CeO_2-TiO_2 catalysts in low-temperature CO oxidation. *Appl. Catal. B. Environ.* 144: 498-506.

Lin, H.K., Chiu, H.C., Tsai, H.C., Chien, S.H. and Wang, C.B. 2003. Synthesis, characterization and catalytic oxidation of carbon monoxide over cobalt oxide. *Catal. Lett.* 88(3-4): 169-174.

Lou, Y. and Liu, J. 2017. CO oxidation on metal oxide supported single Pt atoms: the role of the support. *Ind. Eng. Chem. Res.* 56(24): 6916-6925.

Molavi, R., Safaiee, R., Sheikhi, M.H. and Hassani, N. 2021. Theoretical perspective on CO oxidation over small cobalt oxide clusters. *Chem. Phy. Lett.* 767: 138361.

Panagiotopoulou, P. and Verykios, X.E. 2017. Mechanistic study of the selective methanation of CO over Ru/TiO_2 catalysts: effect of metal crystallite size on the nature of active surface species and reaction pathways. *J. Phys. Chem. C.* 121(9): 5058-5068.

Royer, S. and Duprez, D. 2011. Catalytic oxidation of carbon monoxide over transition metal oxides. *Chem Cat Chem.* 3(1): 24-65.

Schryer, D.R., Upchurch, B.T., Sidney, B.D., Brown, K.G., Hoflund, G.B. and Herz, R.K. 1991. A proposed mechanism for Pt/SnO_x-catalyzed CO oxidation. *J. Catal.* 130: 314-317.

Shao, J.J., Zhang, P., Tang, X.F., Zhag, B.C., Song, W., Xu, Y. and Shen, W.J. 2007. Effect of preparation method and calcination temperature on low-temperature CO oxidation over Co_3O_4/CeO_2 catalysts. *Chin. J. Catal.* 28(2): 163-169.

Tang, C.W., Wang, C.B. and Chien, S.H. 2008. Characterization of cobalt oxides studied by FT-IR, Raman, TPR and TG-MS. *Thermochim Acta.* 473(1-2): 68-73.

Umeshbabu, E., Rajeshkhanna, G., Justin, P. and Ranga Rao, G. 2015. Magnetic, optical and electrocatalytic properties of urchin and sheaf-like $NiCo_2O_4$ nanostructures. *Mater. Chem. Phys.* 165: 235-244.

Valechha, D., Megarajan, S.K., Fakeeha, A.H., Al-Fatesh, A.S. and Labhasetwar, N.K. 2017. Effect of SO_2 on catalytic CO oxidation over nano-structured, mesoporous $Au/Ce_{1-x}Zr_xO_2$ catalysts. *Catal. Lett.* 147(11): 2893-2900.

Vepøek, S., Cocke, D.L., Kehl, S. and Oswald, H.R. 1986. Mechanism of the deactivation of Hopcalite catalysts studied by XPS, ISS, and other techniques. *J. Catal.* 100: 250-263.

Wang, C.B., Tang, C.W., Gau, S.J. and Chien, S.H. 2005. Effect of the surface area of cobaltic oxide on carbon monoxide oxidation. *Catal. Lett.* 101(1-2): 59-63.

Xu, X.L., Sun, X.F., Han, H., Peng, H.G., Liu, W.M., Peng, X., Wang, X. and Yang, X.J. 2015. Improving water tolerance of Co_3O_4 by SnO_2 addition for CO oxidation. *Appl. Surf. Sci.* 355: 1254-1260.

Xu, Z.C., Li, Y.R., Lin, Y.T. and Zhu, T.Y. 2020. A review of the catalysts used in the reduction of NO by CO for gas purification. *Environ. Sci. Pollut. Res. Int.* 27(7): 6723-6748.

Yang, J., Yu, C., Liang, S., Li, S., Huang, H., Han, X., Zhao, C., Song, X., Hao, C., Ajayan, P.M. and Qiu, J. 2016. Bridging of ultrathin $NiCo_2O_4$ nanosheets and graphene with polyaniline: A theoretical and experimental study. *Chem. Mater.* 28(16): 5855-5863.

Yang, Q., Du, L., Wang, X., Jia, C. and Si, R. 2016. CO oxidation over Au/ZrLa-doped CeO_2 catalysts: synergistic effect of zirconium and lanthanum. *Chin. J. Catal.* 37(8): 1331-1339.

Yu, F., Qu, Z., Zhang, X., Fu, Q. and Wang, Y. 2013. Investigation of CO and HCHO oxidation over mesoporous Ag/Co_3O_4 catalysts. *J. Energy Chem.* 22(6): 845-852.

Yu, Y., Takei, T., Ohashi, H., He, H., Zhang, X. and Haruta, M. 2009. Pretreatments of Co_3O_4 at moderate temperature for CO oxidation at - 80 °C. *J. Catal.* 267: 121-128.

Zhang, B.C., Tang, X.L., Li, Y., Cai, W.J., Xu, Y.D. and Shen, W.J. 2006. Steam reforming of bio-ethanol for the production of hydrogen over ceria-supported Co, Ir and Ni catalysts. *Catal. Commun.* 7(6): 367-372.

Zhang, L.L., Sun, M.J. and Liu, C.G. 2019. CO oxidation

on the phosphotungstic acid supported Rh single-atom catalysts via Rh-assisted Mans-van Krevelen mechanism. *Mol. Catal.* 462: 37-45.

Zhang, N., Li, L., Wu, R., Song, L., Zheng, L., Zhang, G. and He, H. 2019. Activity enhancement of Pt/MnO_x catalyst by novel â-MnO_2 for low-temperature CO oxidation: study of the CO-O_2 competitive adsorption and active oxygen species. *Catal. Sci. Technol.* 9: 347-354.

Zhang, X., Dong, H., Wang, Y., Liu, N., Zuo, Y. and Cui, L. 2016. Study of catalytic activity at the Ag/Al-SBA-15 catalysts for CO oxidation and selective CO oxidation. *Chem. Eng. J.* 283: 1097-1107.

Zhang, Y., Wu, Y., Wang, H., Guo, Y., Wang, L., Zhan, W., Guo, Y. and Lu, G. 2015. The effects of the presence of metal Fe in the CO oxidation over Ir/FeO_x catalyst. *Catal. Commun.* 61: 83-87.

Zhong, L.Y., Hai, F., Xiao, P., Hong, J.P. and Zhu, J.J. 2014. Improved low-temperature activity of La-Sr-Co-O nano-composite for CO oxidation by phase cooperation. *RSC Adv.* 4: 61476-61481.

Zhu, Z., Lu, G., Zhang, Z., Guo, Y., Guo, Y. and Wang, Y. 2013. Highly active and stable Co_3O_4/ZSM-5 catalyst for propane oxidation: effect of the preparation method. *ACS Catal.* 3(6): 1154-1164.